JMEPEG (2009) 18:1248–1257
DOI: 10.1007/s11665-009-9385-y

1059-9495/$19.00

The Effect of Ultrasonic Impact Treatment on the Fatigue Resistance of Friction Stir Welded Panels

C.A. Rodopoulos, Sp.G. Pantelakis, and M.P. Papadopoulos

(Submitted December 11, 2008; in revised form January 28, 2009)

In this work, the results of an experimental study for assessing the effects of Ultrasonic Impact Treatment on the fatigue resistance of Friction Stir Welded aluminum alloy panels are presented. Although the significant compressive residual stress introduced on the material by ultrasonic impact treatment (UIT) was expected to cause retardation in the crack growth rate, this was only noted at low initial ΔK values. At high ΔK values, the effect of UIT practically diminishes. The phenomenon was attributed to the relaxation/redistribution of the residual stresses with fatigue damage. This provides an alarming situation where damage tolerance design relies on models where only the initial residual stress profile is taken into account without knowledge of the potential re-distribution of the residual stresses caused by the fatigue damage accumulation. The findings of this work also indicate that any FCG tests performed can only be considered as case-specific and conclusions can only be drawn for the case studied.

Keywords fatigue crack propagation, friction stir welding, relaxation/redistribution of residual stresses, ultrasonic impact treatment

1. Introduction

Commercial transport airplanes generally consist of a built-up metallic structure where the skin-to-stringer, skin-to-clip, and clip-to-frame joints are mostly riveted. Such joints for many years have been the subject of extensive research, especially in terms of multiple site and widespread fatigue damage. The proceedings of the International Conference of Aeronautical Fatigue provide an excellent source for referencing.

Friction stir welding (FSW) is a relatively new process patented by The Welding Institute (Cambridge, UK) in 1992 (Ref 1). A friction stir butt weld is produced by plunging a rotating tool into the facing surfaces of the two plates. The tool consists of a shoulder and a profiled pin emerging from it. As the rotating pin moves along the weld line, the material is heated up by the friction generated by the shoulder and stirred by the rotating pin in a process similar to an extrusion. Since the temperatures are well below the melting point, problems associated with the liquid/solid phase transformation are avoided.

Besides the attractive static mechanical properties such as superior load bearing capacity as compared to riveted joints, FSW integral structures are claimed to offer significant cost and weight savings (Ref 2, 3). Therefore, FSW was recently identified by leading aircraft manufacturers as "key technology" for fuselage and wing manufacturing (Ref 4, 5). Yet, problems associated with the fatigue behavior of FSW are numerous and not yet fully understood.

Generally, FSW produces five distinct microstructural zones (Ref 6) namely, the weld nugget (N), the shoulder contact zone or flow arm region, the thermomechanical-affected zone (TMAZ), the heat-affected zone (HAZ), and unaffected zone or parent plate (PP). Previous work has provided evidence that the cyclic flow resistance of each zone of the welds can significantly vary. Hence, it is rational to assume that the corresponding fatigue strength of FSW joints will vary for each zone of the weld (Ref 7). The FSW weld zone is V-shaped and widens near the top surface due to the close contact between the shoulder of the tool and the upper surface (Ref 8). The above finding indicates potential discontinuities in the strength and fatigue volume properties. Sato et al. (Ref 9) pointed out that the shape of the weld zone depends on the welding parameters and the material used. Dalle Donne et al. (Ref 10) show that with proper FSW tooling and welding parameter control, a reduction of only 20% compared to the base material values for the joint ultimate strength and fatigue endurance can be achieved. In addition, the zones have also been considered responsible for variations in the fatigue failure initiation sites. Booth and Sinclair (Ref 6) identified two forms of failure in the 2024-T351 FSW: (a) failure occurred from within the actual weld material (Nugget) and (b) failure occurred outside of the actual weld, either in the TMAZ or HAZ. Failure within the nugget region was associated with discontinuities in the material flow pattern at the surface. With no obvious defects being seen, the exact origins of crack initiation within this region were not clearly identifiable, while the failure in TMAZ and HAZ initiated by decohesion of large S-phase particles or transgranular failure. They suggest that heterogeneous precipitation at particle interfaces may influence the decohesion strength of the intermetallics at a specific location.

C.A. Rodopoulos, Sp.G. Pantelakis, and **M.P. Papadopoulos**, Laboratory of Technology and Strength of Materials, Department of Mechanical Engineering and Aeronautics, University of Patras, Patras 26500, Greece; and **C.A. Rodopoulos**, Materials and Engineering Research Institute, Sheffield Hallam University, Sheffield S1 1WB, UK. Contact e-mail: m_papado@mech.upatras.gr.

Differences in the quality of the weld are also manifested by the hardness profiling in relation to the five microstructural zones. Jata et al. (Ref 11) reported for the 7050 Al alloy that the hardness of the top side is lower than the bottom side of the weld. They suggested that this is due to the fact that the top side is in full contact with the tool shoulder, and thus, experiences direct heat. The bottom side, on the other hand, is in indirect contact with a back plate that acts as a heat sink. Comparing the hardness between the zones, the hardness within the nugget varies depending on the alloy and its initial heat treatment. For 2024-T351, 7050-7745 and 6061-T6 alloys hardness profiles in the weld nugget show a local maximum value at the plate joint line or center of the nugget (Ref 6, 10, 11). For 6063 Al alloy, the hardness profiles in the weld nugget show a minimum value among other regions. These differences in hardness value within the nugget have been correlated with the size of the precipitates present in the region (Ref 12-15). The 2xxx and 7xxx show the hardness minima within the TMAZ zone (Ref 6, 9, 16, 17). The effect has been attributed to over-aging (Ref 12).

Residual stress fields significantly affect crack nucleation and growth. As stated in Ref 18 and confirmed in Ref 9, 19-21, residual stress distribution varies along the zones of the weld. Webster et al. (Ref 22) measured the residual stresses using Synchrotron x-ray technique and reported tensile residual stress in the nugget zone of 7108-T79. Similar findings were also reported by Bussu and Irving (Ref 12) and Staron et al. (Ref 23) for AA2024-T351, and by Oosterkam et al. (Ref 24) for AA7108-T79. Nevertheless, Jata et al. (Ref 11) and Dalle Donne et al. (Ref 25) found a small compressive residual stress located at the center of the nugget zone for 7050-T7451, Al-Li-Cu, and 6013-T6. Defects associated with the FSW process are strongly associated with fatigue resistance. In Ref 14, 16, 26, it was reported that voids, inclusions, and surface cracks dominate the nugget and represent potential sites for crack initiation.

All this makes it clear that quality process control and fatigue damage tolerance control over FSW joints are a complex requirement demanding extensive and well-organized international research. Yet, driven from today's market and societal needs for prompt innovation, cost and pollutant emission reduction (Ref 27), the fatigue behavior of FSW joints needs to be improved and safeguarded. Such solution can be sought in terms of surface engineering treatments.

The ultrasonic impact treatment (UIT) (Ref 28) is a technique that directly deforms the surface of materials using ultrasonic impacts. This technique fundamentally differs from contact methods of ultrasonic deformation treatment, the development of which dates back to 1950s (Ref 29). The UIT process employs continuous ultrasonic vibrations at the ultrasonic transducer output end strengthened with hard materials (carbide-containing alloys, artificial diamonds, etc.) and in direct and generally continuous contact with the treated surface. The process is mainly controlled by the output of the ultrasonic transducer (frequency), the selected pressure, the feed rate, and the number of passes (coverage). The process can induce on request different amounts of cold work and residual stress profiles. The depth of the latter can range from 0.8 to 4 mm in aluminum alloys (Ref 30). The process is relatively cheap compared to controlled shot peening and can achieve process rates in excess of 300 mm/min.

In this work, the potential of using UIT in order to increase the crack growth resistance of FSW panels is investigated. Testing has been performed on specimens with and without UIT treatment. In order to evaluate the stability of the treatment, different initial ΔK values were implemented. The tests were performed on specimens large enough as to ensure that there is no internal stress relief caused by specimen cutting and preparation. Extensive metallographic investigation and residual stress measurements have been performed to support the investigation.

2. Experimental Procedure

2.1 Material, Specimens, and Testing

The investigation was performed on a 13-mm-thick 2024-T351 FSW joint. The joints were provided by Airbus UK, Broughton. Plates, 13 mm thick, have been welded along their long edge with the weld direction parallel to the longitudinal (rolling) orientation. The welds were produced using a spindle speed of 200 rpm and a feed rate of 120 mm/min. The chemical composition and basic static mechanical properties of the parent material are shown in Tables 1 and 2, respectively.

For identification and measurement of the five zones microstructure, the weld was cross-sectioned using a Beuhler

Table 1 Chemical composition of 2024-T351 in wt.% based on EDX measurements

Alloy	Si	Fe	Cu	Mn	Mg	Cr	Zn	Ti	Zr	Al
2024-T351										
Min	...	...	3.8	0.30	1.2	...	...	...	...	Balance
Max	0.50	0.50	4.9	0.90	1.8	0.10	0.25	0.15	...	

Table 2 Basic mechanical properties of 2024-T351 according to ASTM E8 m-94a

Mechanical properties	Mean	99% Conf.	Std. dev	Std. err
0.2% Yield strength, MPa	347.0	5.1	4.6	1.5
Tensile strength, MPa	484.7	2.6	2.3	0.8
Elongation, %	15.0	0.2	0.2	0.1
Fracture toughness – plane stress, MPa $\sqrt{m}$, for thickness 1.6 mm	135.6	8.7	3.0	1.5
Strain energy density, MJ/m^3	70.5	0.6	0.6	0.2

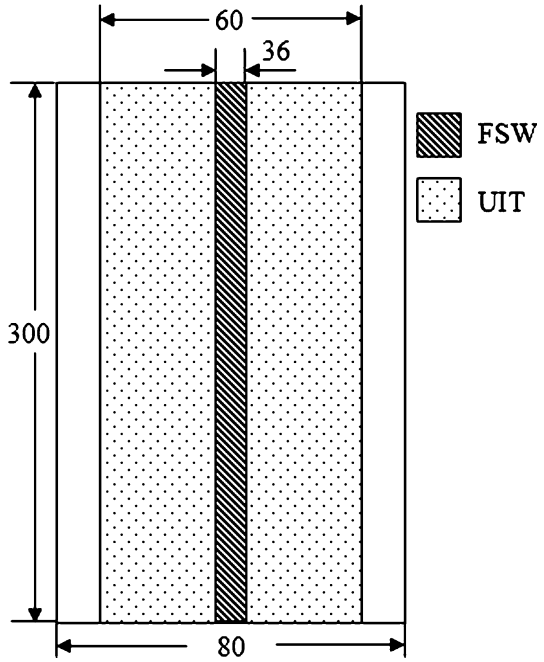

Fig. 1 Testing panel's configuration (not to scale)

Isomet 4000 precision diamond saw with rotational disk speed of 4100 rpm and a feed rate of 1.6 mm/min. The sections underwent mechanical polishing using a series of emery papers and diamond pastes until a ¼ μm finish was reached. To reveal the microstructure, the sections were etched using Keller's reagent in accordance with ASTM E340-00.

To investigate possible alterations in the nature of Cu precipitates due to the welding process, etching of the top surface at different locations was prepared by sputtering erosion (using argon ion) using a glow discharge optical emission spectrometer (GDOES), LECO GDS-750 QDP, operating at voltage 600 V, and current 25 mA. The etched spots (4 mm in diameter) were later used for back scattered scanning electron microscopy.

Residual stress measurements were performed using Incremental Hole-Drilling according to ASTM E837-99. Prior to drilling, a 0.5-mm layer was milled to remove the onion ring scar. This is a common practise in order to minimize surface stress concentrations. All measurements have been performed at a depth of 0.1 mm and represent near surface conditions.

Finally, UIT treatment was performed on Single Edge Notch panel specimens having the weld line perpendicular to the notch. Figure 1 depicts the specimen design. The 2 mm initial slit was introduced using electro-discharge machining. All testing panels were treated according to the parameters shown in Table 3. The panels prior to treatment were cleaned in nitride-free detergent and degreaser suitable for aerospace components. Cleaning is imperative to prevent any residues from machining and handling entering the surface. Uniform clamping of the panels was performed using a vacuum table. The exerted clamping pressure was 72 MPa. The UIT treatment parallel to the weld line was performed. The treatment was conducted at a distance of ±30 mm from plate joint line (PJL).

In order to develop a fatigue crack from the slit, an initial stress of 200 MPa was initially selected followed by load shedding similar to that used in the determination of crack growth threshold. Load shedding was designed in order to deliver a crack of length 4 mm at an initial ΔK value of 4, 8, and 14 MPa $\sqrt{m}$. The value of 4 MPa $\sqrt{m}$ is representative of the long crack threshold ΔK of the parent material. The case supports the following rationale. Since the FSW could include areas of lower long crack threshold ΔK values, it is necessary to make sure that the ΔK of the induced-crack in the testing article is not high enough as to prevent initiation of cracking from such areas. In other words, the potential development of additional fatigue damage within the FSW area is not excluded. The other testing parameters were: stress ratio 0.1, frequency 20 Hz, temperature 19 °C, and humidity 48%. Crack growth measurements were performed via a high-resolution camera and in-house dedicated software. Similar testing setup was used in the case of the UIT-treated specimens. Two tests were performed for each initial ΔK value, both for the untreated- and the UIT-treated specimens.

Table 3 UIT *Esonix* process parameters

Carrier frequency, kHz	36
Pin dimension, mm	∅6.3 × 17, R25, Titanium
Normalized impact	64 impulses
Amplitude under load, μm	12
Pressure, kg	15
Impact frequency, Hz	36
Tool overlapping rate, %	50
Coverage, %	200
Feed rate, mm/min	150

3. Results and Discussion

3.1 Weld Micromechanical Properties and Mapping

Figure 2 shows the grain size distribution of the different zones. The nugget exhibits the finest grain with sizes in the range between 5 and 10 μm. The flow arm zone was found to have a fine-equiaxed grain structure of approximately 15 μm. The TMAZ exhibits a nonuniform and severely elongated microstructure. The elongated grain size is found to range between 200 and 400 μm representing different degrees of thermomechanical plastic deformation which governed the amount of material drawn into the weld zone. The grain structure in HAZ and in the parent plate appears to have similar size in the order of 150-200 μm. The process also allowed the detailed 2D mapping of all the different zones as shown in Fig. 3. The PJL corresponds to the center weld section and is being used as scaling origin. The map also reveals the nonsymmetrical distribution of the zones left or right to the PJL with the right TMAZ showing smaller area compared to its left counterpart. Such discrepancy is attributed to contact pressure difference in the disc shoulder (possibly during rotation).

The hardness profiles measured along the top and bottom surface of the specimens are shown in Fig. 4. In general, the hardness of the bottom surface is lower than that at the top. This is particularly the case for the nugget zone (flow arm for the top surface). The lowest hardness value from the top surface, approximately $118Hv_{10}$, was found in the TMAZ and especially closer to the interface with the HAZ (13 mm from the PJL). In contrast, the bottom surface exhibited its lowest microhardness value within the nugget and TMAZ zone (approximately

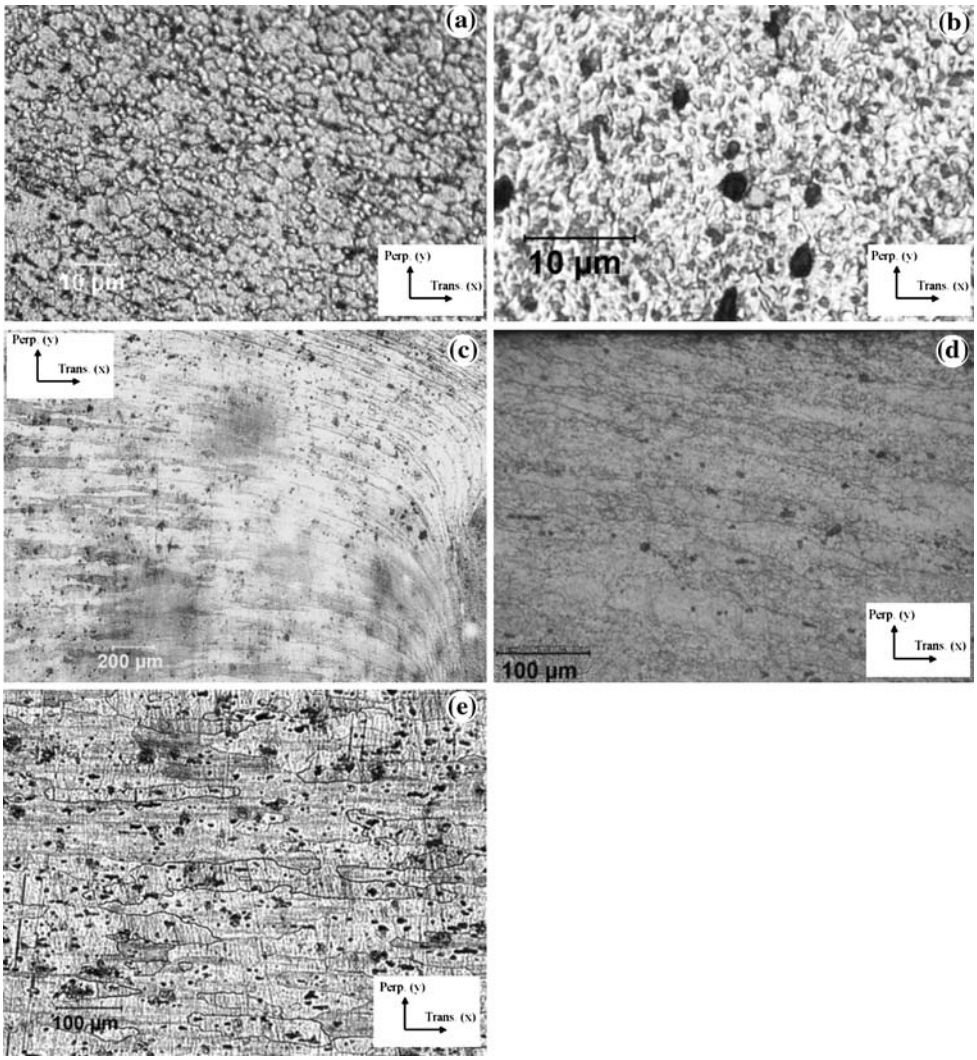

Fig. 2 Grain structure distribution exhibited within the five zones

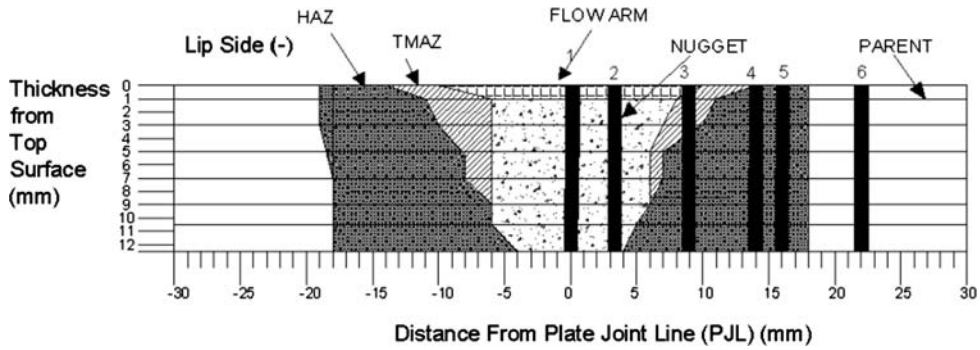

Fig. 3 Two-dimensional mapping of the weld

105-118Hv_{10}). The highest top surface microhardness value of 167Hv_{10} was found within the HAZ (approximately 16 mm from the PJL). Similar results can also be confirmed for the bottom surface.

In order to investigate the variation of the gradient of the thermomechanical plastic deformation taking place during the welding process, which, as previously shown is manifested by differences between the top and bottom weld surface, through thickness microhardness measurements were taken from six selected sections (see Fig. 3). The measurements are depicted in Fig. 5.

To better acknowledge the tendencies, regression analysis was performed. The analysis reveals that: (a) section 1 (nugget) exhibits degradation of its microhardness value with depth at a

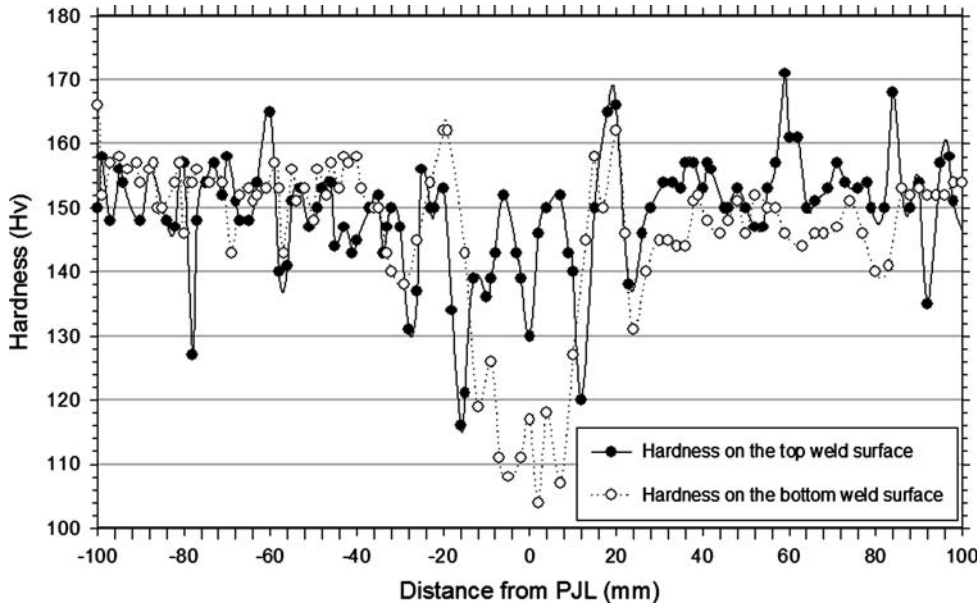

Fig. 4 Vickers hardness distribution across the weld surface. A 10-kg load was used

rate of 1.4 Hv/mm; (b) section 2 exhibits similar behavior to section 1 at a rate of 0.78 Hv/mm; (c) section 3 (TMAZ + HAZ) demonstrates minimum microhardness growth at a rate of 0.42 Hv/mm. Herein it is important to note that the transition from TMAZ to HAZ at a depth of approximately 3.2 mm did not register any significant change; (d) section 4 (HAZ close to TMAZ) shows significant increase in the microhardness with a growth rate of 0.85 Hv/mm; (e) section 5 (clear HAZ) shows significant increase at a rate of 1.35 Hv/mm, and finally (f) section 6 (clear parent) shows trivial increase at a rate of 0.21 Hv/mm.

Figure 6(a) shows two images taken from the PJL zone. The low magnification image reveals that Cu precipitates exhibit a nonuniform distribution and are concentrated at the interfaces between finer and coarser grains (being the result of unsuitable cooling). The high magnification image reveals broad size distribution of the precipitates (between 0.1 to 1.5 μm). Figure 6(b) shows that at the right hand side of the weld (+) and at a distance of 2 mm, precipitates are still agglomerated. Precipitate agglomeration is a typical feature of the rolling process that the plate underwent prior to FSW. Such feature disappears at a distance of ±5 mm. Significant grain size variations and strong agglomeration of precipitates have also been found in the TMAZ, as shown in Fig. 6(c). The black spots have been identified by EDX as K, Si, and Cl oxides. The HAZ, Fig. 6(d), shows significant coarsening and more uniform distribution of the precipitates as well as elongated microstructure. It is worth noting that K and Mn oxides were traced only on the left hand side of the weld. The above changes are better appreciated by comparison to the parent material shown in Fig. 6(e).

The results of the residual stress measurements are shown in Fig. 7. They indicate that: (a) the nugget is in compression with values reaching maxima close to PJL; (b) the TMAZ is also in compression but with a tendency to achieve tension; (c) the HAZ is generally in tension with maxima found at the transition location between TMAZ and HAZ. Single edge notch crack growth specimens were milled with dimensions according to Fig. 1. The 2 mm initial slit was introduced using electro-discharge machining. Prior to testing and in order to identify potential redistribution of the residual stresses due to the manufacturing of the testing article, the residual stresses were measured once again at the selected locations. The results, Fig. 7, indicate that machining did not produce any significant alteration in the residual stress distribution close to the surface. As such it is rational to assume that the selected testing article dimensions are not subjected to scale effects.

3.2 Fatigue Crack Growth Behavior

Figure 8 shows the experimental results of the FCG tests, both for the untreated specimens as well as for the specimens after UIT treatment for the three selected cases. From the results, the following comments can be made: (a) at low stress levels and low initial stress intensity factor (SIF) (4 MPa $\sqrt{m}$), the effect on the UIT can lead to significant benefit. However, such potential increase in fatigue resistance gradually diminishes with increasing applied stress and high initial SIF (14 MPa $\sqrt{m}$); (b) the initial compressive residual stress field induced by the treatment does not significantly affect long crack growth (crack length >10 mm); and (c) significant increase at low stress levels is found in the area where the UIT has reversed the sign of the residual stresses (TMAZ).

In order to identify the role of the residual stresses during fatigue damage (redistribution), hole-drilling measurements were performed at different locations from the crack tip at the crack plane. The results for the case of the as-received and the UIT-treated testing articles with initial ΔK values of 4, 8 MPa $\sqrt{m}$ are shown in Fig. 9 and 10, respectively. From the results, it can be seen that propagation of the crack causes severe redistribution of the residual stresses. The results indicate that redistribution is higher from the side of crack growth (negative to PJL) while the magnitude increases with the far-field stress.

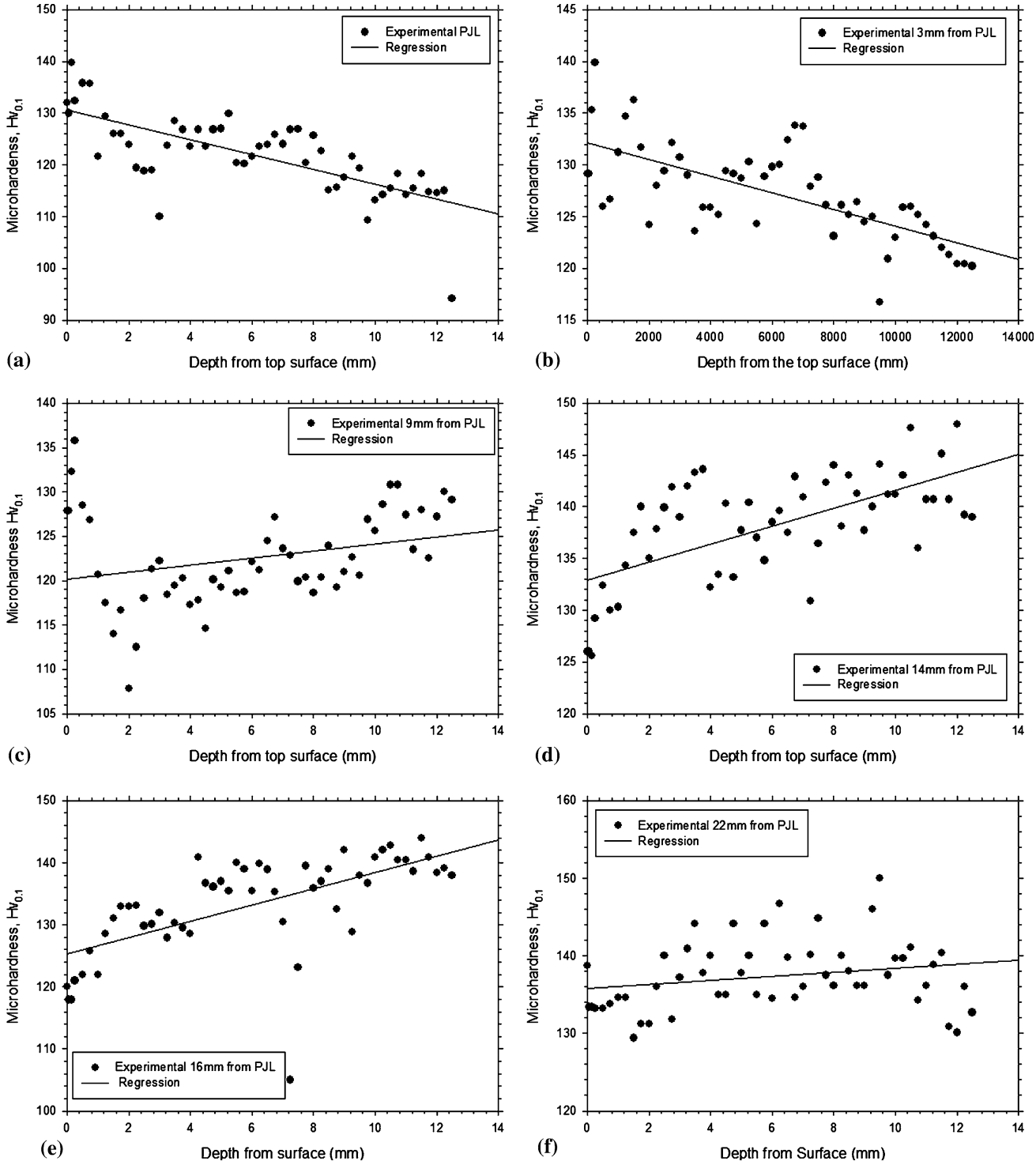

Fig. 5 Microhardness measurements along the six selected sections

4. Conclusion

The work represents an initial application of the technology of UIT in an attempt to improve the crack growth resistance of friction stir welds. The results indicate that the technology can change the sign of the residual stresses from tension to significant compression. In principle, such change is considered as beneficial to crack growth resistance if the concept of the effective stress range or effective stress ratio is acknowledged. Yet, crack growth tests at different far-field stresses shown that such potential is subjected to both the size of the crack and the corresponding far-field stress level. This is due to the significant re-distribution of the residual stresses which is evident in both the cases of as-received and UIT-treated testing article.

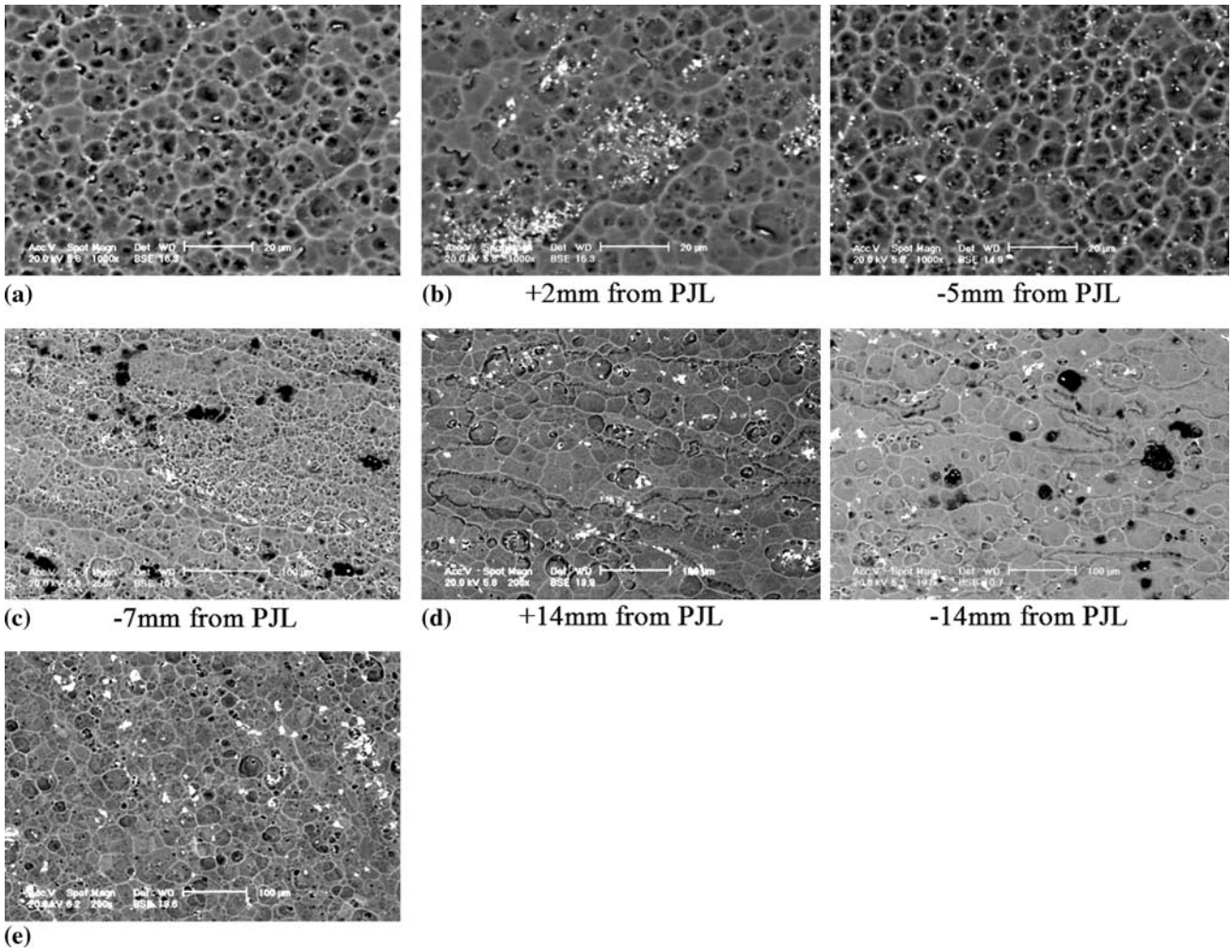

Fig. 6 Back scattered images taken from GDOES prepared spots at different locations as well as from the left (−) or right (+) side of the weld

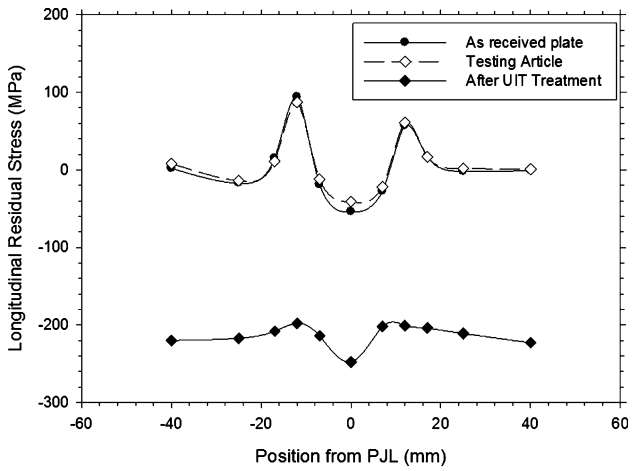

Fig. 7 Near surface residual stress distribution for as-received, after machining, and after UIT treatment

In addition, it can be easily seen that regarding to the value of ΔK, the redistribution of the residual stresses as well as the corresponding crack growth rate may differ.

The generated problem is best described if the principle of similitude is engaged. Herein, the concept that long cracks will deliver similar propagation rate under the same ΔK values cannot be applied either in models where the effective stress range or the effective stress ratio is used without taking into account the dynamic relaxation/redistribution of the residual stresses. This is due to the progression of fatigue damage imposed by the far-field stress, being mainly affected by the number of cycles and its maximum value. Herein, fatigue damage is associated with cyclic plasticity during the early fatigue stages and to crack growth with progressing number of fatigue cycles. The nature of the latter is twofold, namely, the cracked volume which dynamically reduces the available material for accommodating residual stresses and second, the crack-tip plasticity volume which is residual stress free. As a result, it is rational to assume that linear elastic solutions should not be applied unless they are able to encapsulate the above.

This provides an alarming situation where damage tolerance design relies on models where only the initial residual stress profile is taken into account without knowledge of the potential re-distribution of the residual stresses caused by the far-field stress, the crack initiation site, and the selected geometry to accommodate the above findings.

The findings of this work also indicate that any FCG tests performed can only be considered as case-specific and conclusions can only be drawn for the case studied. In other words, it is imperative, prior to any investigation, to ascertain that the

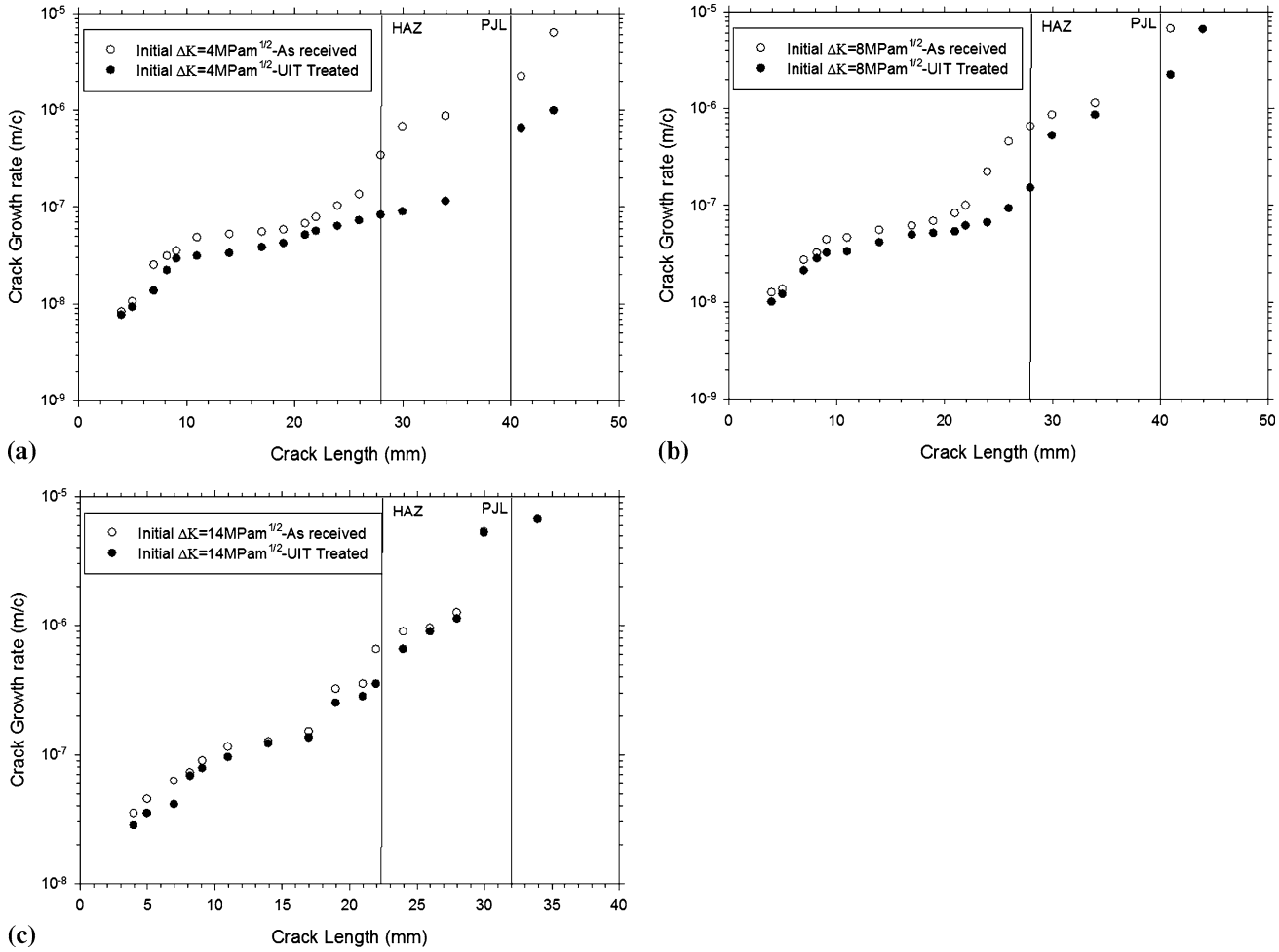

Fig. 8 Experimental results (crack growth rate vs. crack length) for the three selected testing cases (a-c)

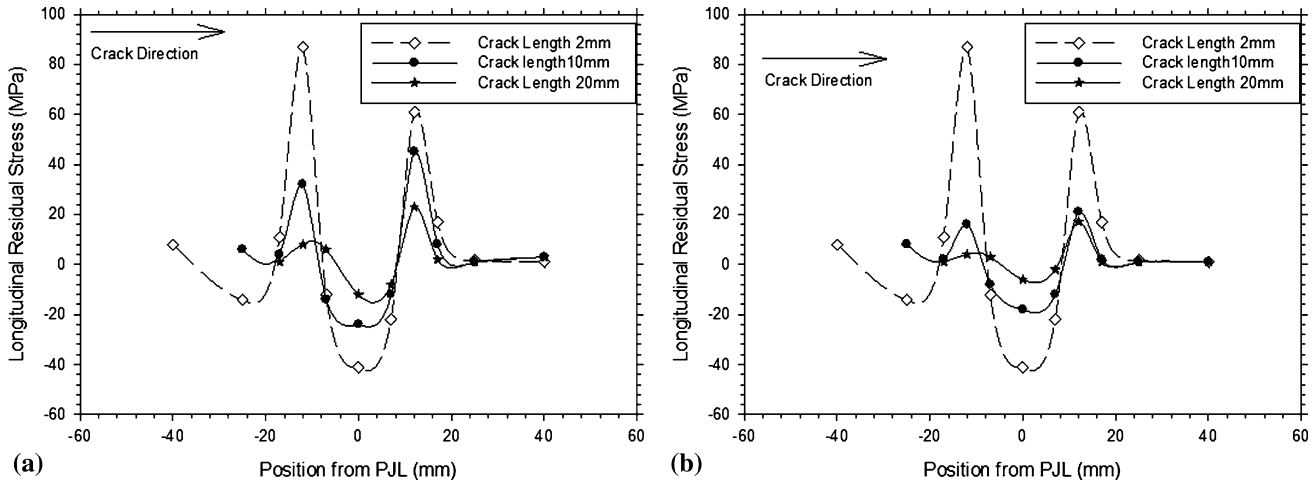

Fig. 9 Redistribution of residual stresses in the as-received specimens with crack position for the case of an initial ΔK value of (a) 4 MPa $\sqrt{m}$ and (b) 8 MPa $\sqrt{m}$

testing article remains representative of the residual stress profile of the full scale component and consider that (a) the far-field stress will provide an initial relaxation/redistribution of the residual stress profile and (b) crack propagation will alter the above profile in a way that the correction factors used for determining ΔK are not valid. The reader should also keep in mind that the findings of this work represent a unique case so in terms of the FSW parameters as well as the UIT treatment.

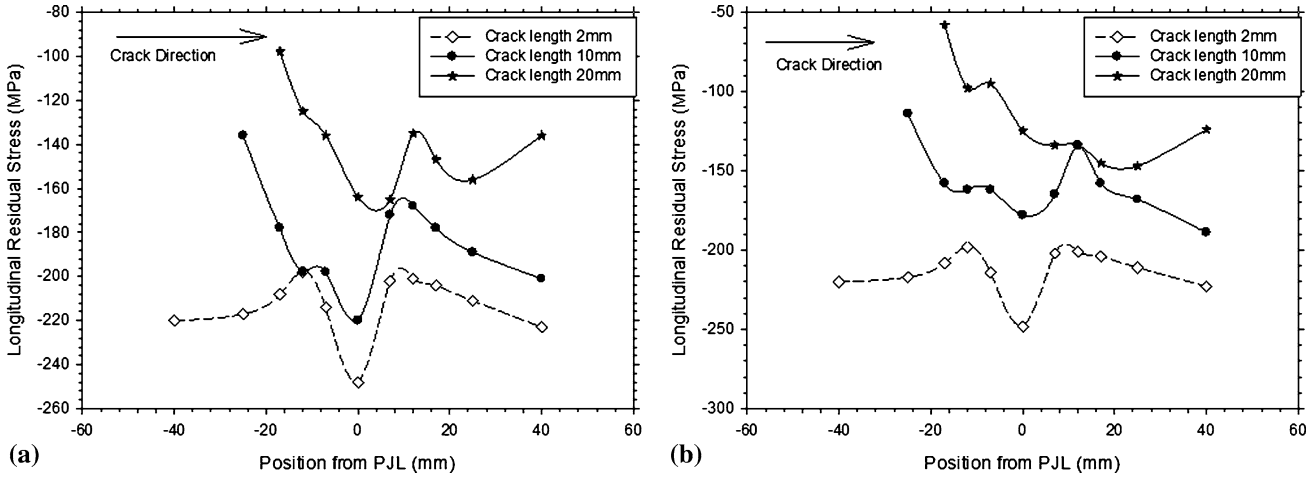

Fig. 10 Redistribution of residual stresses in UIT-treated specimens with crack position for the case of an initial ΔK value of (a) 4 MPa $\sqrt{m}$ and (b) 8 MPa $\sqrt{m}$

There is no indication that the relaxation/redistribution will remain similar if other parameters had been used. Therefore, it is rational to support that the problem of addressing fatigue damage in unstable residual stress fields is complex and requires knowledge, which at this stage has not been properly accumulated. As such, it is realistic to assume that damage tolerance evaluation of FSW components should be treated as case-specific, until all parameters which could affect the stability of the residual stresses, i.e., FSW parameters, material microstructural features, surface treatments, component dimensions, etc. can be accounted in such a way as to reflect potential interactions.

Acknowledgments

The work was financial supported by Airbus UK and Applied Ultrasonics Inc.

References

1. W.M. Thomas, E.D. Nicholas, J.C. Needham, M.G. Murch, P. Templesmith, and C.J. Dawes, "Improvements Relating to Friction Welding," European Patent EP 0 615 480 B1, 1992
2. M. Hansen, A Cooler Weld, Mechanical Engineering, *Design Supplement*, 2003, www.memagazine.org/medes03/coolweld/coolweld.html
3. R.G. Pettit, J.J. Wang, and C. Toh, "Validated Feasibility Study of Integrally Stiffened Metallic Fuselage Panels for Reducing Manufacturing Costs," NASA/CR-2000-209342, 2000
4. R. Talwar, D. Bolser, R. Lederich, and J. Baumann, Friction Stir Welding of Airframe Structures, *Second International Symposium on Friction Stir Welding*, TWI, UK, 2000
5. D. Lohwasser, Welding of Airframes by Friction Stir, *Third International Symposium on Friction Stir Welding*, TWI, UK, 2001
6. D. Booth and I. Sinclair, Fatigue of Friction Stir Welded 2024-T351 Aluminium Alloy, *J. Mater. Sci. Forum*, 2002, **396–402**, p 1671–1676
7. A. Ali, X. An, C.A. Rodopoulos, M.W. Brown, P. O'Hara, A. Levers, and S. Gardiner, The Effect of Controlled Shot Peening on the Fatigue Behaviour of 2024-T3 Aluminium Friction Stir Welds, *Int. J. Fatigue*, 2007, **29**(8), p 1531–1545
8. B. Heinz, B. Skrotzki, and G. Eggeler, Microstructural and Mechanical Characterization of a Friction Stir Welded Al-Alloy, *J. Mater. Sci. Forum*, 2000, **331–337**, p 1757–1762
9. Y.S. Sato, S.H.C. Park, and H. Kokawa, Microstructure Factors Governing Hardness in Friction Stir Welds of Solid Solution Hardened Al Alloys, *J. Metall. Mater. Trans. A Phys. Metall. Mater. Sci.*, 2001, **32A**(12), p 3033–3042
10. C. Dalle Donne and G. Biallas, Fatigue and Fracture Performance of Friction Stir Welded 2024-T3 Joints, *Proceeding European Conference on Spacecraft Structure, Material and Mechanical Testing*, Vol. 1, Braunschweig, Germany, 1999, p 309–314
11. K.V. Jata, K.S. Sankaran, and J.J. Ruschau, Friction Stir Welding Effects on Microstructure and Fatigue of Aluminium Alloy 7050-T7451, *J. Metall. Mater. Trans.*, 2000, **A31**(9), p 2181–2192
12. G. Bussu and P.E. Irving, The Role of Residual Stress and Heat Affected Zone Properties on Fatigue Crack Propagation in Friction Stir Welded 2024-T351 Aluminium Joints, *Int. J. Fatigue*, 2003, **25**, p 77–88
13. L. Murr, Y. Li, E.A. Trillo, R.D. Flores, and J.C. McClure, Microstructure in Friction Stir Welded Metals, *J. Mater. Process. Manuf. Sci.*, 1998, **7**, p 145–161
14. Y.S. Sato and H. Kokawa, Distribution of Tensile Property and Microstructure in Friction Stir Weld of 6063 Aluminium, *Metall. Mater. Trans. A*, 2001, **32A**(12), p 3023–3031
15. O.V. Flores, C. Kennedy, L.E. Murr, D. Brown, S. Pappu, B.M. Nowak, and J.C. McClure, Microstructural Issues in a Friction Stir Welded Aluminium Alloy, *Scripta Mater.*, 1998, **38**(5), p 703–708
16. G. Bussu, "Damage Tolerance of Welded Aluminum Aircraft Structure," Ph.D. Thesis, Cranfield University, 2000
17. C.G. Rhodes, M.W. Mahoney, and W.H. Bingel, Effect of Friction Stir Welding on Microstructure of 7075 Aluminium, *Scripta Mater.*, 1997, **36**(1), p 69–75
18. K. Masubuchi, *Analysis of Welded Structures*, Pergamon Press, Oxford, UK, 1980
19. M. Ericsson and R. Sandstrom, Fatigue of Friction Stir Welded AlMgSi-Alloy 6082, *Mater. Sci. Forum*, 2000, **331–337**, p 1787–1792
20. J.A. Esparza, W.C. Davis, E.A. Trillo, and L.E. Murr, Friction Stir Welding of Magnesium Alloy AZ31B, *J. Mater. Sci. Lett.*, 2002, **21**, p 917–920
21. M.W. Mahoney, C.G. Rodes, J.G. Flintoff, R.A. Spurling, and W.H. Bingel, Properties of Friction Stir Welded 7075 T651 Aluminium, *Metall. Mater. Trans. A*, 1998, **29A**, p 1955–1964
22. P.J. Webster, L.D. Oosterkam, P.A. Browne, D.J. Hughes, W.P. Kang, P.J. Withers, and G.B.M. Vaughan, Synchrotron X-Ray Residual Strain Scanning of a Friction Stir Weld, *J. Strain Anal.*, 2001, **36**(1), p 61–70
23. P. Staron, M. Koçak, S. Williams, and A. Wescott, Residual Stress in Friction Stir-Welded Al Sheets, *J. Physica B Condens. Matter*, 2004, **350**(1–3, Suppl 1), p E491–E493
24. L.D. Oosterkam, P.J. Withers, P.A. Browne, and G.B.M. Vaughan, Residual Stress Field in a Friction Stir Welding Aluminium Extrusion, *Mater. Sci. Forum*, 2000, **347–349**, p 678–683

25. C. Dalle Donne, E. Lima, J. Wegener, A. Pyzalla, and T. Buslaps, Investigations on Residual Stress in Friction Stir Welds, *Third International Symposium on Friction Stir Welding*, Sept 27-28, 2001 (Kobe, Japan), TWI, UK, 2001
26. C. Dalle Donne, G. Biallas, T. Ghidini, and G. Raimbeaux, Effect of Weld Imperfections and Residual Stresses on the Fatigue Crack Propagation in Friction Stir Welded Joints, *Second International Conference on Friction Stir Welding*, June 26-28, Gorthenburg, Sweden, 2000
27. Strategic Research Agenda, Advisory Council for Aeronautics Research in Europe, Vol. 2, October 2004, Available at: http://www.acare4europe.org/html/documentation.asp
28. C.A. Rodopoulos, J.S. Romero, S.A. Curtis, E.R. de Los Rios, and P. Peyre, The Effect of Controlled Shot Peening and Laser Shock Peening on the Fatigue Performance of 2024-T351 Aluminium Alloy, *Mater. Eng. Perf.*, 2003, **12**(4), p 414–419
29. S.A. Curtis, E.R. de los Rios, C.A. Rodopoulos, J. Solis Romero, and A. Levers, Investigating the Effects of Controlled Shot Peening on Corrosion Fatigue, *Eighth ICSP*, L. Wagner, Ed., Wiley VCH, 2003, p 264–270
30. E.Sh. Statnikov, V.N. Vityazev, and O.V. Korolkov, Study of Comparative Characteristics of Ultrasonic Impact and Optimization of Deformation Treatment Processes, *Fifth World Congress on Ultrasonics*, Paris, France, 2003